Composites Part B 231 (2022) 109546

Contents lists available at ScienceDirect

Composites Part B

journal homepage: www.elsevier.com/locate/compositesb

# Development of bi-directional pseudo-ductile glass/carbon-epoxy hybrid composites for improved safety in structural applications

Gergely Czél

*Department of Polymer Engineering, Faculty of Mechanical Engineering, Budapest University of Technology and Economics, Műegyetem rkp. 3, H-1111, Budapest, Hungary*

ARTICLE INFO

*Keywords:*
A. Hybrid
A. Carbon fibre
A. Glass fibre
D. Mechanical testing
Fragmentation

ABSTRACT

Pseudo-ductility was demonstrated in interlayer hybrid composites which have fibre reinforcement in two perpendicular directions. The central carbon-epoxy layer was reinforced with a range of fibres either in balanced spread tow tape based dry fabric or unidirectional prepreg format oriented in 0° and 90°. The high strain S-glass/epoxy layers were made of the same unidirectional prepregs with 0/90° orientation for all tested configurations. Stiffness increments of 20–70% were achieved compared to the estimated elastic modulus of the cross-ply S-glass/epoxy baseline composite. Pseudo-ductile stress-strain response with visually detectable damage initiation and a plateau after the initial linear stage was obtained for all configurations. The manufacturing of the developed laminates was found to be suitable for an industrial setting with no need for special equipment.

## 1. Introduction

Fibre reinforced composites are among the best choices for weight-critical applications such as aerospace and motorsports for decades for their outstanding specific mechanical properties. Fatigue and corrosion resistance also contribute to their success, decreasing the lifetime cost of components and structures. However, the failure of composites is usually catastrophic without sufficient warning and residual load-bearing, in line with the general strength-ductility trade-off dilemma of structural materials [1–4]. The sudden and therefore undesirable failure of high performance composites is usually compensated for by cautious design allowables [5]. This way, the potential of the outstanding structural properties of composites is not fully exploited. Pseudo-ductile, high performance composites failing in a safe and progressive manner showing highly non-linear stress-strain response and detectable damage, which can serve as a warning sign before final failure, are therefore of high interest.

The most straightforward approach to address the brittle failure of thermoset polymer matrix fibre reinforced composite materials is to replace their intrinsically brittle constituents with more ductile ones. Toughening of the matrix material has a limited effect on the fibre-dominated lamina properties, but it can have a larger impact on laminate level damage tolerance, e.g. by improving the delamination resistance. A well-established concept is to add rubber and/or thermoplastic particles to the thermoset matrix (typically epoxy) to increase its toughness. More recently, nanoscale additives such as carbon nanotubes and graphene nano-platelets were found to be effective in toughening the matrix of composites [6–9]. This latter approach increased the mode I interlaminar fracture toughness [8] under quasi-static loading and decreased the delamination crack propagation rate under fatigue loading [9]. Improved matrix properties may be obtained by hybridisation of thermoset resins as well, especially if co-continuous interpenetrating network structure is achieved [10]. Electrospun nanofiber veils as a targeted modification to the composite ply interfaces were also applied successfully for toughening [11–15]. However, high throughput electrospinning methods suitable for producing quantities sufficient to cover large areas with the nanofibrous mats are still under development [16,17]. High stiffness and strength yet ductile fibres have even more potential than new matrix materials, but their development is an extremely challenging (e.g. due to the strength-stiffness trade-off) and rather long process. Nevertheless, promising results were presented, e.g. with nanotube fibres [18], regenerated cellulose [19] and other polymeric fibres in the last decade. At the moment, these new ductile fibres cannot provide elastic moduli and strength values comparable to those of traditional glass or carbon fibres. The only high performance fibres showing excellent intrinsic ductility, which was successfully transferred to their polymer matrix composites as well, are made of stainless steel [20–23]. However the high steel fibre volume fraction composites have a relatively high density which may limit their application in weight-critical applications.

*E-mail address:* czel@pt.bme.hu.

https://doi.org/10.1016/j.compositesb.2021.109546
Received 8 June 2021; Received in revised form 5 August 2021; Accepted 28 November 2021
Available online 3 December 2021

In the last decade, pseudo-ductility was achieved by carefully designing the architecture of composite laminates made of conventional constituents to allow for deformations higher than the failure strain of the fibres and highly non-linear stress-strain response with warning before final fracture. The most successful approaches include angle-ply composites where the fibres can re-orient towards the loading direction [24–26], discontinuous composites at the fibre [27,28] and the lamina [29] level offering deformation potential beyond the failure strain of the fibres and hybridisation of different fibres in the same matrix (i.e. fibre hybrid composites).

Fibre hybrid composites can be produced in different ways [2], generally aiming at progressive damage process with final failure at higher deformation than the ultimate strain of the stiffer fibres in the hybrid. A new class of the most straightforward interlayer (or sandwich) hybrids was developed recently using thin carbon fibre reinforced plies together with standard thickness S-glass reinforced plies to generate pseudo-ductility through the fragmentation and stable delamination of the thin central carbon layer [30]. The concept was demonstrated with the hybridisation of different modulus carbon fibres as well [31], showing favourable stress-strain responses with a plateau after the initial linear rise, which can serve as a warning before final failure. The first laminate architectures were unidirectional (UD) for both glass/-carbon and carbon/carbon hybrids, then pseudo-ductility was confirmed for more complicated quasi-isotropic (QI) lay-up sequences as well [32,33]. A unique intrinsic damage visualisation feature of the fragmenting glass/carbon hybrid laminates by the development of a unique striped pattern beyond the failure strain of the carbon fibre reinforced layer was also demonstrated and patented [34,35].

This study aims to develop structural materials with safe, progressive (i.e. pseudo-ductile) failure mode and damage visualisation feature, which are more suitable for real applications than UD hybrid laminates, by providing load-bearing capacity in more than just one direction. Applying novel high performance constituents such as woven spread tow tapes, which have not been proposed earlier, and adapting the available analytical design formulae to bi-directional architectures, a new family of pseudo-ductile hybrid composites are presented. The new bi-directional hybrids offer superior scope for structural applications, due to their more balanced load-bearing capacity, compared to UD hybrids, at the cost of slightly more complicated structure. On the other hand the bi-directional hybrids are still simpler to manufacture than the QI hybrids, which in return have further benefits in balanced load-bearing. Therefore the targeted bi-directional pseudo-ductile composites are considered as a promising intermediate solution between UD and QI hybrids, widening the selection of pseudo-ductile hybrid composites for design engineers. Revealing the structure-property relations is also a key target of the study. Therefore the role of the fragmenting block thickness in the resulting tensile stress-strain response of some of the proposed new materials is analysed and discussed in detail. Exploiting the unique damage visualisation feature of glass-carbon hybrid laminates for further safety improvement is also an excellent opportunity to make the new materials more attractive to designers of structural components.

## 2. Design

This section provides information about the concept, the laminate design and the materials utilised during the development of the pseudo-ductile hybrid composites.

### 2.1. Concept

The motivation for developing this new family of hybrid composites was primarily the issue that despite their excellent longitudinal performance, the penetration of unidirectional (UD) pseudo-ductile hybrid laminates into many structural applications may still be hindered due to their poor transverse mechanical properties. On the other hand, the complicated structure of quasi-isotropic (QI) hybrids [32,33] limits their minimum thickness and increases their manufacturing (i.e. cutting and lay-up) cost. As a mechanically suitable but simple to manufacture compromise between UD and QI hybrid laminates, various bi-directional reinforcement structures inc. thin spread tow tape based fabrics and cross-ply sub-laminates with thin fragmenting plies were considered. The ultimate aim was to extend the scope of pseudo-ductile composites with new types which provide good mechanical properties in two directions but can still be manufactured with reduced cost due to their simple structure.

In order to realise the desired simple bi-directional structures, UD and fabric type carbon fibre reinforcements were combined with UD glass reinforcement in various balanced and symmetric interlayer hybrid lay-up sequences always containing the same amount of each type fibres in both 0° and 90° directions. Fig. 1 shows the schematic of the specimen geometry and structure.

The carbon/glass fibre volume ratios and the full thickness of the low strain material (LSM) were set according to previously published criteria [30] for fragmentation of the central carbon layer and stable delamination around the fractures in the carbon layer. This way, the typical major load-drop at the fracture of the LSM in the hybrid laminates can be avoided, and a slightly rising plateau can be generated instead, with further rise after complete fragmentation of the LSM (Fig. 2.).

### 2.2. Materials

The materials considered for design and used for the experiments were thin carbon/epoxy prepregs from SK Chemicals made of TC35 type high strength (HS) carbon fibres and K50 type general purpose epoxy resin. Other two carbon fibre types: Mitsubishi's MR70 type intermediate modulus (IM) and HS40 type high modulus (HM) carbon fibres were utilised in a thin spread tow dry fabric format (TeXtreme) manufactured by Oxeon from 20 mm wide tapes (see Fig. 3.). These thin, dry fabric plies were impregnated either with resin from the neighbouring thicker glass/carbon UD prepreg plies or with thin epoxy resin films inserted between the thin, dry fabric plies. There was no suitable high strength glass fabric structure available for the study. Therefore, UD S-glass/epoxy prepregs made by Hexcel with 913 epoxy resin were used in cross-ply stacking sequences as the high strain material (HSM) of the hybrid laminates. Both resins in the prepregs (913 and K50) were cured at 125 °C and found compatible, although the suppliers provided no details on their chemical formulations. The good integrity of the hybrid laminates was confirmed during test procedures. Basic properties of the applied fibres and prepreg systems can be found in Tables 1 and 2.

### 2.3. Hybrid laminate design

The following design criteria were identified earlier [31] to assure stable pseudo-ductile failure for UD interlayer hybrids:

1) The outer HSM layers (see Fig. 1) need to be thick and strong enough to take the entire load after LSM fracture and (stable or unstable) delamination. Inequality (1) is useful for choosing the HSM for a

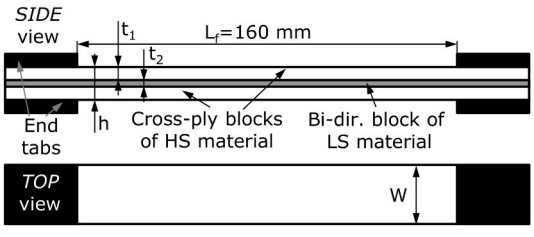


**Fig. 1.** Specimen design schematic (HS- high strain, i.e. glass/epoxy, LS- low strain, i.e. carbon/epoxy).

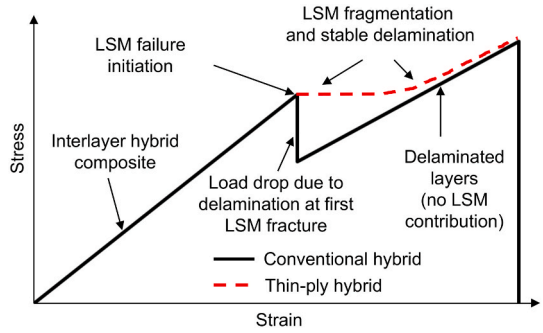


**Fig. 2.** Schematic of the stress-strain response of conventional and thin-ply interlayer hybrid composites (LSM-low strain material).

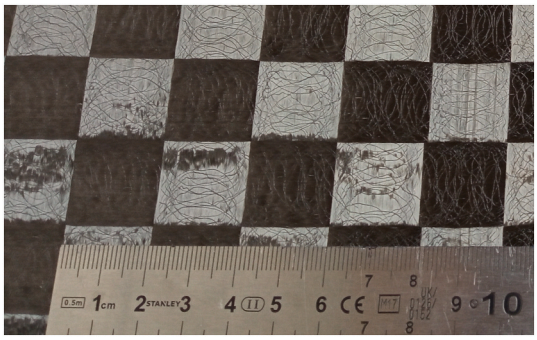

**Fig. 3.** Image of a TeXtreme spread tow tape carbon fibre fabric with a unit cell size of approx. 20 mm. (Random patterns on the UD carbon fibre tapes correspond to the thermoplastic scrim fibres.)

selected LSM by giving the HSM's minimum required strength for given layer thicknesses and initial moduli.

$$\sigma_{1b} > \frac{\sigma_{2b}(2E_1t_1 + E_2t_2)}{2E_2t_1} \tag{1}$$

Where $E_1$ is the elastic modulus of the HSM layers in the loading direction, $E_2$ is the elastic modulus of the LSM layer in the loading direction, $t_1$ is the thickness of one HSM layer, $t_2$ is the thickness of the LSM layer as shown in Fig. 1, $\sigma_{1b}$ is the breaking stress of the HSM layers in the loading direction, $\sigma_{2b}$ is the breaking stress of the LSM layer in the loading direction.

Inequality (1) can be rearranged in another form which is more practical for stacking sequence design. Inequality (2) gives the minimum thickness of one HSM layer ($t_1$) for a given material pair and LSM thickness required to avoid premature failure at LSM layer fracture.

$$t_1 > \frac{\varepsilon_{2b}E_2t_2}{2E_1(\varepsilon_{1b} - \varepsilon_{2b})} \tag{2}$$

Where $\varepsilon_{1b}$ and $\varepsilon_{2b}$ are the breaking strains of the HSM and LSM layers in the loading direction, respectively. If, as a first approximation, the breaking strains of the composite layers are estimated by the fibre failure strains, a lower bound for the HSM layer thickness can be obtained. A sufficient margin should be allowed to account for stress concentration in the HSM layer due to the LSM layer fracture and gripping effects, which was not considered in this simple design approach.

2) The energy release rate ($G_{II}$) at the expected failure strain (fibre failure strain as a first approximation) of the LSM layer must be lower than the mode II fracture toughness ($G_{IIC}$) of the interface (approximately 1 N/m$^2$ based on previous measurements) to avoid catastrophic delamination of the central LSM layer after its first fracture. This criterion assures the condition for fragmentation and stable delamination of the LSM layer.

$$G_{II} = \frac{\varepsilon_{2b}^2E_2t_2(2E_1t_1 + E_2t_2)}{8E_1t_1} < G_{IIC} \tag{3}$$

The criteria above, initially formulated for UD fibre architectures, were adapted to the new bi-directional reinforcement structures by calculating the elastic modulus of the bi-directionally reinforced blocks of carbon/epoxy and glass/epoxy separately in the following way:

a) Cross-ply sequence of UD prepreg plies: The rule of mixtures (Voigt model) and the inverse rule of mixtures (Reuss model) was utilised to determine the elastic moduli of the longitudinally and the transversely oriented UD plies, and they were homogenised through their loading direction stiffnesses (thickness*unit width*elastic modulus). Since all tested configurations had the same amount of fibres in 0° and 90°, this operation was simplified to averaging the

**Table 1**
Properties of the applied fibres based on manufacturer's data (HS- high strength, IM-intermediate modulus, HM-high modulus).

| Fibre type | Manufacturer | Elastic modulus | Strain to failure | Tensile strength | Density |
|---|---|---|---|---|---|
| | | [GPa] | [%] | [GPa] | [kg/m$^3$] |
| Y-110 S-2 Glass | AGY | 89 | 5.7 | 4.89 | 2470 |
| Tairyfil TC35 carbon | Formosa Plastics | 240 (HS) | 1.6 | 4.0 | 1800 |
| Pyrofil MR70 carbon | Mitsubishi Rayon | 324 (IM) | 2.2 | 7.0 | 1820 |
| Pyrofil HS40 carbon | Mitsubishi Rayon | 425 (HM) | 1.1 | 4.61 | 1850 |

**Table 2**
Cured ply properties of the applied materials (UD -unidirectional).

| Material designation | Manufacturer | Structure | Nominal fibre areal density[a] | Fibre volume fraction[a] $V_f$ | Cured ply thickness[c] | UD elastic modulus[c] | Bi-directional block elastic modulus[c] |
|---|---|---|---|---|---|---|---|
| | | | [g/m$^2$] | [%] | [μm] | [GPa] | [GPa] |
| S-glass/epoxy | Hexcel | UD prepreg | 190 | 51 | 154 | 46.1 | 26.1 |
| TC35/epoxy | SK Chemicals | UD prepreg | 20 | 40 | 27.8 | 98.0 | 51.8 |
| MR70 | Oxeon | dry fabric | 42 | ~50[b] | 46.2 | 163.7 | 85.2 |
| HS40 | Oxeon | dry fabric | 43 | ~50[b] | 46.5 | 214.2 | 110.5 |

[a] Based on the manufacturer's data.
[b] Approximate value for design purpose only.
[c] Estimated using manufacturer's data.

longitudinal and transverse elastic moduli of the carbon/epoxy and the glass/epoxy layers, respectively.

b) Thin spread-tow dry fabric architecture: The fabric was decomposed into longitudinally and transversely oriented UD plies with thicknesses half of the fabric ply. The longitudinal and transverse elastic moduli of these UD plies were averaged similarly to the cross-ply UD case.

This way, formulae (2) and (3) can be applied in the same form, just the material properties have to be updated according to the reinforcement architecture. The failure strains of the bi-directional blocks were still estimated by the fibre failure strains for simplicity. The minimum thickness of the HSM was checked for all designed configurations, and I found, that the actual thickness of the HSM layers was more than five times the calculated minimum thickness in all cases. Therefore all configurations passed criterion 1) with a large margin for effects not considered in the design calculation. The $G_{II}$ values of the designed configurations are calculated by assuming a fragmenting block including all LSM plies of all orientations and the neighbouring 90° oriented HSM plies, as only 0° oriented HSM plies are expected to stop the developing through-thickness fractures of the carbon/epoxy layer during the fragmentation process. Fig. 4 shows the possibility of different volume fragmenting blocks formed in the same hybrid lay-up sequence through the example of the TC35 carbon/S-glass hybrid configuration tested in 0° and 90° loading directions. In all the considered carbon spread tow tape fabric LSM hybrids (see Table 3.), the HSM plies adjacent to the fragmenting carbon/epoxy LSM layer are 90° oriented. Therefore these plies are included in the fragmenting block for $G_{II}$ prediction, assuring a conservative design. However, if the laminates would have been loaded in 90° direction, these HSM plies would not fragment, and the resulting $G_{II}$ would be significantly lower. Due to the fabric structure of the LSM not being sensitive to the loading direction and since material availability was limited, these configurations were only tested in the more critical 0° direction.

The $G_{II}$ values predicted at LSM layer fracture are included in Table 3 and they are all below the estimated $G_{IIC}$ (1 N/mm), meaning that fragmentation and stable delamination of the LSM block is expected for all designed configurations. In addition to the standard checks, a few intentions were implemented in the selected configurations according to the design formulae. (i) A significant difference between the failure strain of the HSM and LSM is preferred for a wide plateau in the stress-strain curve before final failure. This is the reason for using high failure strain S-glass/epoxy as HSM for the hybrid laminates instead of lower strain E-glass/epoxy. (ii) Maximum allowable LSM/full thickness ratio is targeted for high initial stiffness, stress plateau and elastic-plastic style response in all configurations. That is the reason for testing the more conservative *1HS40* and the more critical *2HS40* hybrid laminates with a higher LSM/full thickness ratio as well. Table 3 shows the selected configurations and the results of the design calculations.

## 3. Experimental

This section presents the manufacturing process of the coupons, the methods and equipment applied for mechanical testing and the discussion of the results obtained.

### 3.1. Specimen geometry

The specimens tested within the study were parallel edge end-tabbed tensile specimens. Nominal specimen dimensions were 260/160/W/h overall length, free length in mm, variable width and thickness, respectively (see Fig. 1.). The width of the specimens made of UD plies was 20 mm, but the ones made of spread tow tape fabrics needed to be higher, to include minimum 2 unit cells, therefore it was selected to be 40 mm. Specimen fabrication was done carefully, not to follow the tape boundaries with the cutting lines.

### 3.2. Specimen manufacturing

According to the given lay-up sequences, the hybrid laminates specified in Table 3 were prepared by hand lay-up technique from 300 × 300 mm pre-impregnated (prepreg) and dry fabric sheets. For the configurations containing only one single dry fabric, no additional resin was used as the excess resin in the relatively thick glass/epoxy plies was expected to impregnate the thin, dry carbon fabrics. However, a 34 GSM epoxy film (made of the same 913 epoxy as the matrix of the prepreg plies) was applied for the configuration containing two plies of dry HS40 carbon fabric to avoid insufficient impregnation and dry spots in the laminate. During the lay-up of the *2HS40 fabric* configuration, attention was paid to offset the fabric plies in both in-plane directions by 10 mm (half of the unit cell size) to avoid unexpected damage due to the interference of the tape boundaries of the fabric plies. The laminates were then put on a flat aluminium tool plate and covered with 2 mm thick silicon sheets, vacuum distributing fleece and a vacuum bag in preparation for autoclave curing. The silicon sheets allowed uniform pressure distribution on the laminates while providing a smooth surface. All plates were cured at 125 °C and 0.7 MPa for 90 min which was suitable for both applied prepreg systems according to the manufacturers' instructions. The resulting thickness of the plates were very close to the nominal ones (the largest deviation was 3%), therefore the test results were evaluated based on the nominal thicknesses. The individual specimens were cut from the 300 × 300 mm cured composite plates with a diamond cutting wheel to the desired overall length and width. Finally, 50 mm long tabs of glass mat/unsaturated polyester were bonded to the ends of the specimens with Araldite 2011 (Huntsman) type two-part epoxy adhesive after degreasing and roughening the bonding surfaces.

### 3.3. Mechanical test procedure

Testing of the parallel edge hybrid composite coupons was executed under uniaxial quasi-static tensile loading and displacement control at a crosshead speed of 2 mm/min on a computer-controlled Zwick Z250

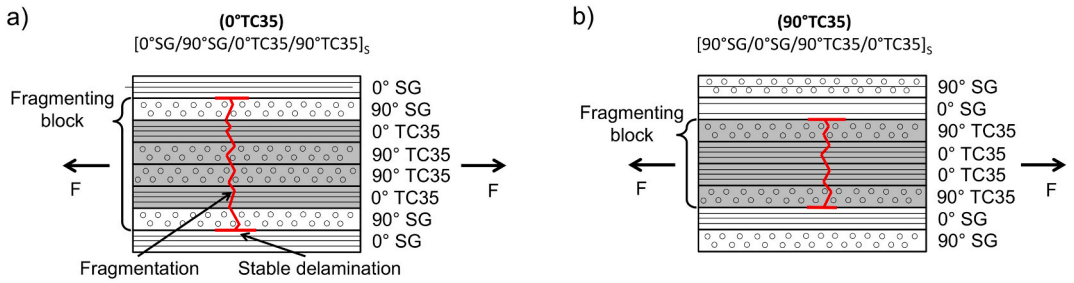


**Fig. 4.** Schematic of the fragmenting block of the TC35 carbon/S-glass hybrid configuration tested in 0° and 90° orientation (SG- S-glass, subscript *s* indicates mid-plane symmetry).

**Table 3**
Specimen types selected for testing. (SG -S-glass. Subscripts indicating the number of plies in a block are only added where multiple plies were stacked together. Subscript *s* indicates the symmetry of a laminate sequence to the mid-plane. LSM-low strain material. The fragmenting blocks of the TC35 configurations are marked with bold and underlined font.)

| Hybrid configuration (Abbreviation) [Lay-up sequence] | Fibre areal densities of the constituent plies [g/m$^2$] | Nominal thickness $h$ [mm] | LSM layer/full thickness ratio [%] | Calculated $G_{II}$ at LSM nominal failure strain [N/mm] | Predicted elastic modulus [GPa] |
|---|---|---|---|---|---|
| **(MR70 fabric)** [0°SG/90°SG/MR70/90°SG/0°SG] | [190/190/42/190/190] | 0.662 | 7.0 | 0.985 at 2.2% | 30.2 |
| **(1HS40 fabric)** [0°SG/90°SG/HS40/90°SG/0°SG] | [190/190/43/190/190] | 0.662 | 7.0 | 0.315 at 1.1% | 32.0 |
| **(2HS40 fabric)** [0°SG/90°SG/HS40$_2$/90°SG/0°SG] | [190/190/86/190/190] | 0.708 | 13.1 | 0.680 at 1.1%[a] | 37.2 |
| **(0° TC35 UD)** [0°SG/**90°SG/0°TC35/90°TC35**]$_S$ | [190/190/20/20]$_S$ | 0.727 | 15.3 | 0.748 at 1.6% | 30.0 |
| **(90° TC35 UD)** [90°SG/0°SG/**90°TC35/0°TC35**]$_S$ | [190/190/20/20]$_S$ | 0.727 | 15.3 | 0.501 at 1.6% | 30.0 |

type 250 kN rated universal electro-mechanic test machine fitted with a regularly calibrated 250 kN load cell and 100 kN rated Instron 2716–003 type manual wedge action grips. The strains were measured optically on one side of the specimens, with a Mercury Monet type video-extensometer using an approx. 110 mm gauge length and white markers (made with sharp tip paint marker) on a black background (made with blunt tip permanent marker) for high contrast.

The stress-strain curves of the tested hybrid laminates were evaluated according to Fig. 5 to determine the first knee point of the diagrams by fitting lines on the sections before and after the pseudo-yield point. Since the scope of the study was the plateau in the stress-strain response, a number of the tests were stopped before the final failure of the specimens to preserve them for further damage analysis. Therefore the final strain in the stress-strain diagrams should not be considered as failure strain. Five specimens were tested from all configurations, except for the *1HS40 fabric* type, where only four valid tests were executed.

### 3.4. Results and discussion

The pseudo-ductile stress-strain curves of the ***MR70 fabric*** specimen series can be seen in Fig. 6. The diagrams show a significant reduction of slope around 1.76% strain (see Table 4 for details) which is called the pseudo-yield point where extensive fragmentation of the LSM (i.e. carbon/epoxy) layer in the hybrid laminate took place. The pseudo-yield stress is just below 500 MPa, which is respectable for a structural material of less than 2000 kg/m$^3$ density. The obtained pseudo-yield strain (1.76%) is significantly lower than the failure strain of the MR70 fibres (2.2%), but a notable reduction was expected due to additional, concentrated bending stresses induced at the cross-over lines of the thin carbon fibre tapes of the fabric structure. If we re-calculate the $G_{II}$ for the actual pseudo-yield point, we can understand why the plateau is steeper than expected: The moderate $G_{II}$ = 0.63 N/mm re-calculated for the experimental pseudo-yield strain (1.76%) (see

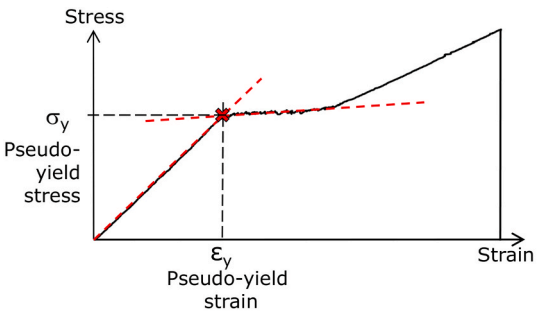


**Fig. 5.** Schematic of the evaluation of the pseudo-yield point on a typical stress-strain curve of a pseudo-ductile hybrid composite.

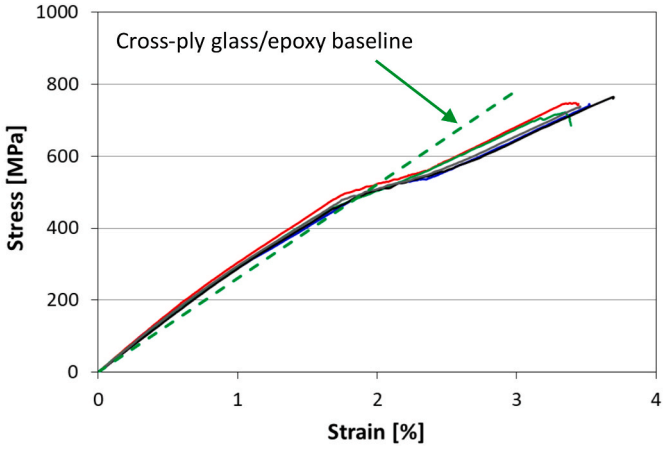


**Fig. 6.** Stress-strain diagrams of the ***MR70 fabric*** type carbon/glass-epoxy interlaminar hybrid specimen series made with intermediate modulus, high strain carbon fabric. The predicted linear stress-strain response of the cross-ply glass/epoxy layers is included as a baseline.

Table 4.) is far from the critical value (approx. 1 N/mm), and therefore local delaminations around the fractures were suppressed in the hybrid laminates during the carbon layer fragmentation process. This relatively low available strain energy level limited the reduction of the tangent modulus of the material during the first half of the plateau. Additional energy from further overall stress increase was required to make the mode II delamination cracks propagate, which led to a stress plateau initially steeper than expected. This phenomenon was observed earlier in UD glass/carbon-epoxy hybrid laminates when very thin carbon plies were applied [30,36]. The early fractures probably around the cross-over points in the carbon fabric were followed by fractures in the flat regions, where higher local failure strains are expected. This reinforcement structure induced dispersion of the in-situ failure strain of the carbon/epoxy layer could have contributed to the development of a significantly rising plateau. Having a close look at the test curves, we can confirm that the slopes of the plateaus gradually decrease right until the second knee point corresponding to fragmentation saturation, which is in line with the increase of the $G_{II}$ with overall strain. This means that if the fragmentation had started at higher GII (i.e. higher strain) as predicted based on the properties of the fibres, the plateau would have been flatter. Cautious laminate design (i.e. considering higher fragmentation strain for the carbon/epoxy layer) resulted in (i) moderate elastic modulus increment (21.2%) introduced by the single, thin fragmenting carbon fabric ply and (ii) limited plateau width.

Fig. 7 shows typical images of damaged hybrid specimens capturing their full 160 mm free lengths after tests interrupted before final failure

**Table 4**
Summary of the test results (the coefficient of variation- CoV values in relative % are given in brackets after the average values).

| Laminate configuration | Predicted elastic modulus | Measured elastic modulus[a] (CoV) | Modulus increase to nominal glass/epoxy | Pseudo-yield strain (CoV) | Pseudo-yield stress[a] (CoV) | Updated $G_{II}$ at pseudo-yield strain |
|---|---|---|---|---|---|---|
| | [GPa] | [GPa] | [%] | [%] | [MPa] | [N/mm] |
| MR70 fabric | 30.2 | 31.6 (4.13) | 21.2 | 1.76 (6.22) | 480.2 (4.54) | 0.631 |
| 1HS40 fabric | 32.0 | 36.4 (8.59) | 39.6 | 0.99 (9.99) | 320.0 (8.51) | 0.256 |
| 2HS40 fabric | 37.2 | 44.7 (7.16) | 71.3 | 0.95 (6.99) | 390 (5.30) | 0.507 |
| 0° TC35 UD | 30.0 | 34.9 (1.77) | 33.7 | 1.63 (4.33) | 511 (4.09) | 0.777 |
| 90° TC35 UD | 30.0 | 34.7 (3.76) | 33.2 | 1.80 (2.60) | 553 (2.65) | 0.634 |

[a] Evaluated with the nominal thickness.

to preserve the specimens for further analysis. The dense striped pattern of the ***MR70 fabric*** specimen corresponds to the fragmentation of its LSM layer and local delaminations around the periodic fractures. This unique damage visualising feature of glass/carbon hybrid laminates can be highly beneficial for safety-critical structural applications and can be further exploited for damage and overload indication, as discussed in Ref. [34]. There is a line along the loading direction in the middle of the first specimen in Fig. 7 where the visible stripes (i.e. cracks and delaminations) are not continuous. This denotes the edges of the spread-tow tapes the carbon fabric is made of. Although similar lines

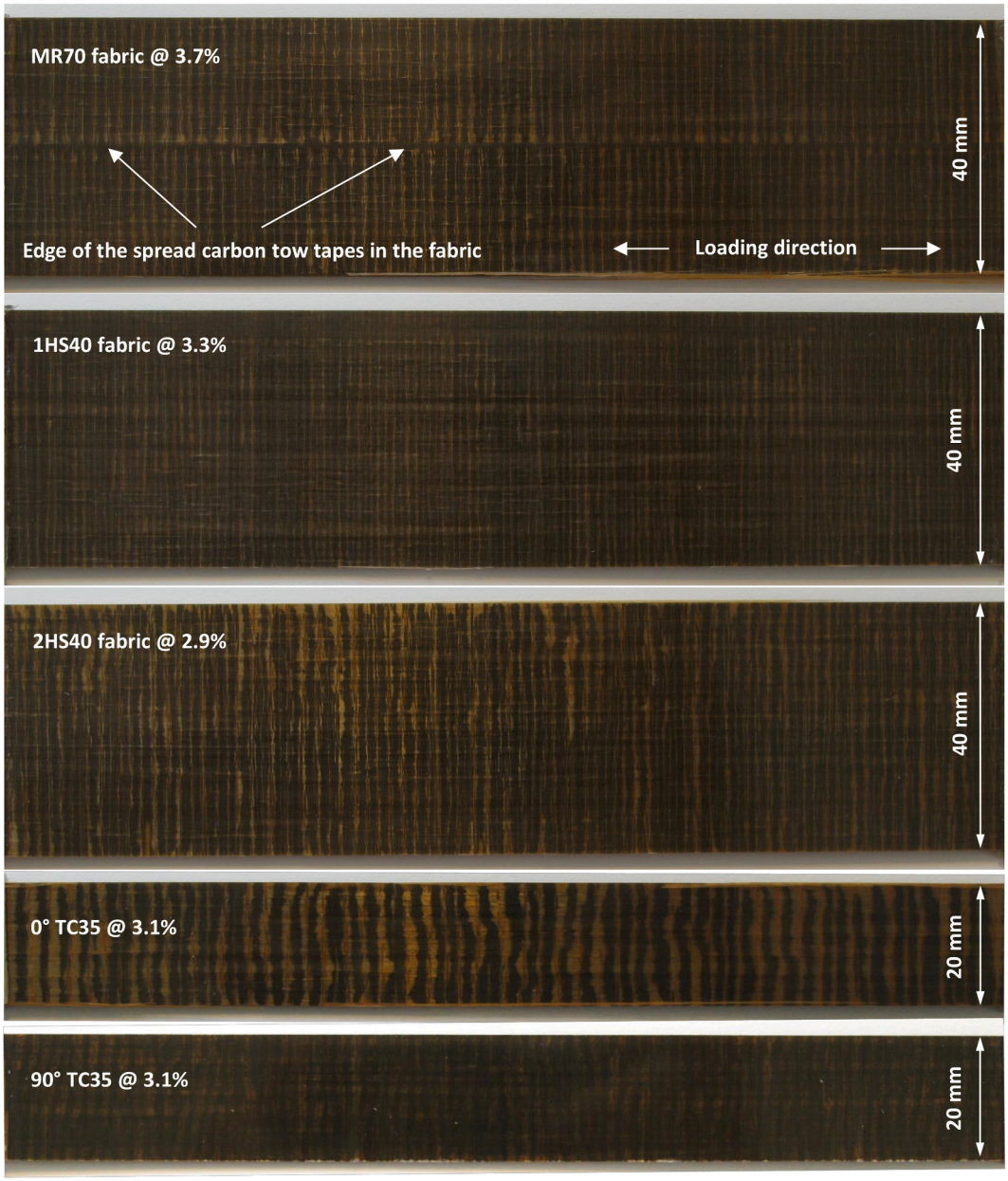


**Fig. 7.** Images of different type carbon/glass-epoxy interlaminar hybrid specimens taken after tests interrupted at strain values indicated after the specimen type designations in the figure.

were well visible on other spread tow tape fabric-based hybrid specimens as well, no splitting or other local damage compromising the integrity of the laminates was detected around these features in any case.

Fig. 8 shows the pseudo-ductile stress-strain curves of the configurations made with HS40 high modulus carbon fibre fabric plies as the LSM. The ***1HS40 fabric*** configuration shows a lower initial slope due to having only one ply of high stiffness LSM in the hybrid laminate. This rather conservative laminate design also resulted in limited stiffness increment (32%) provided by the small amount of LSM (the LSM/full thickness ratio is only 7%) and lower plateau stress, but a slightly higher pseudo-yield strain than those of the ***2HS40 fabric*** configuration.

The latter was most probably due to the hybrid effect shifting the damage initiation point towards higher strains in case of very low energy released by the fractures of thin LSM layers in interlaminar hybrids, as discussed in Ref. [37]. The short plateau had a significantly rising shape for similar reasons as in the ***MR70 fabric*** case: Delamination was highly suppressed by the low $G_{II} = 0.256$ N/mm (Table 4.). On the other hand, the higher LSM/full thickness ratio (up to 13%) in the ***2HS40 fabric*** specimens allowed for a more than 70% elastic modulus increase in the hybrid laminate compared to the pure S-glass/epoxy composite and higher plateau stress of up to 400 MPa. The slightly earlier damage (i.e. fragmentation) initiation is attributed to the higher energy release rate due to the thicker LSM layer. Both specimen types provided a visual indication of damage in the form of a striped pattern revealing the periodic LSM fractures and the localised delaminations around them (see Fig. 7). The developed pattern was more pronounced but less dense in the case of the ***2HS40 fabric*** configuration, again due to the higher amount of energy released upon LSM fractures, which became available to drive longer local delaminations around the fragmentation cracks.

Fig. 9 shows the stress-strain curves of the configurations based on UD high strength carbon/epoxy prepregs as the LSM. The difference between the ***0° TC35 UD*** and ***90° TC35 UD*** types is only the loading direction compared to the reference axis of the lay-up sequence. Both plates were manufactured with entirely identical lay-up sequences, but one of the cured hybrid laminates were turned in-plane by 90° before cutting the tensile test specimens. For simplicity, the lay-up sequences in Fig. 4 and Table 3 are given in reference coordinate systems where the *x*-axes are aligned with the direction of the external load applied during the uniaxial tensile tests. Both ***TC35 UD*** laminates showed favourable pseudo-ductile failure character regardless of the loading direction (see Fig. 9.). The average pseudo-yield strain of the ***0°TC35 UD*** series corresponding to damage initiation was lower (1.63% vs 1.80% for the ***90°*** version), most probably because the fragmenting block of this

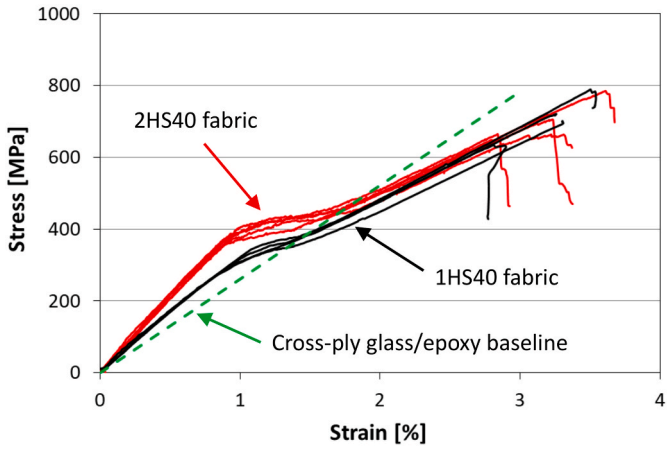


**Fig. 8.** Stress-strain diagrams of the ***1HS40 fabric*** and ***2HS40 fabric*** type carbon/glass-epoxy interlaminar hybrid specimen series made with high modulus carbon fabric. The predicted linear stress-strain response of the cross-ply glass/epoxy layers is included as a baseline.

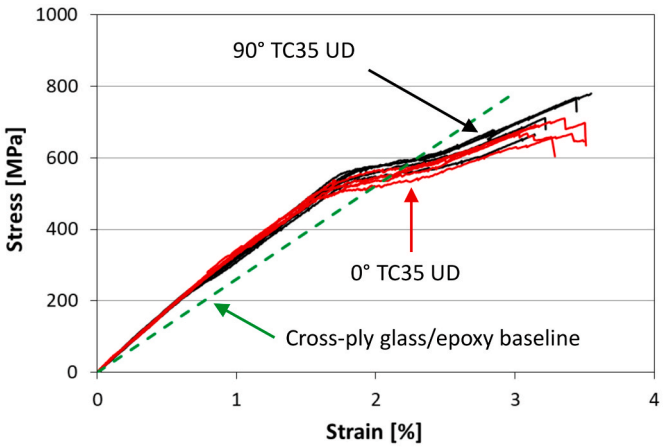


**Fig. 9.** Stress-strain diagrams of the ***0° TC35 UD*** and ***90° TC35 UD*** type carbon/glass-epoxy interlaminar hybrid specimen series made with high strength unidirectional carbon/epoxy prepreg. The predicted linear stress-strain response of the cross-ply glass/epoxy layers is included as a baseline.

hybrid laminate included one 90° oriented glass/epoxy ply on each side of the carbon layer, in contrast to the ***0°TC35 UD*** coupons. The extra energy released by the relatively thick, transversely oriented glass/epoxy plies (see $G_{II} = 0.777$ vs 0.634 N/mm in Table 4.) promoted earlier delamination onset between the fragmenting block and the outer 0° glass/epoxy plies.

This way, the laminate stiffness was reduced earlier, which resulted in a slightly earlier knee point on the stress-strain curves (see Fig. 9.). Similar elastic moduli, 33% higher than that of the glass/epoxy baseline and respectable pseudo-yield stresses above 500 MPa (see Table 4.) were achieved for both UD TC35 carbon ply based specimen types. However, the manufacturing of thin, UD carbon/epoxy ply based hybrid laminates was more laborious than that of the dry fabric based ones. Both laminates showed excellent damage indication ability, especially the ***0°TC35 UD*** type (see Fig. 7.), where the energy available for delamination at carbon/epoxy layer fracture was higher, promoting a less dense, but more pronounced fragmentation pattern by more delamination around the fractures. Better contrast was also observed, as the delaminating interface was closer to the surface of the specimens, right under just one 0° glass/epoxy ply.

Investigating the results summary given in Table 4 it is worth noticing that the predicted and experimentally determined elastic moduli of the series did not match completely, which could have been due to the very simple inverse rule of mixtures being applied to estimate the elastic properties of the transversely oriented layers. The measured moduli were evaluated based on the nominal thicknesses of the specimen types, which matched well with the measured average thicknesses of the series with less than 3% maximum deviation. The elastic modulus increment achieved by hybridisation ranged from 20 to 70%, which provides freedom for designers to tailor the structure and the properties of the pseudo-ductile hybrid composites to the application. The usual trade-off between the elastic modulus and the damage initiation strain was present in the tested configurations, with the stiffest hybrids having a knee point on their stress-strain curve relatively early, but in turn, these types (with high modulus HS40 carbon fibres) provided the widest safety margin between detectable damage initiation and final failure. The high strain carbon (i.e. MR70 and TC35) based configurations provided moderate modulus increment but significantly higher damage initiation strain and pseudo-yield stresses above 500 MPa. The $G_{II}$ values re-calculated for the actual damage initiation strains instead of the nominal carbon fibre failure strains were lower than the values used at the design stage (see Table 4.), which indicate that the tested configurations were conservative and there is still some space for improving the performance of the hybrid laminates and assessing more critical designs.

Currently, the thermal residual strains were not evaluated because reliable thermal expansion coefficients for all the constituent materials were not available, and a reasonable but straightforward estimation approach to the thermal strains of the fabric-based plies is yet to be developed. The few presented configurations indicate the design freedom and safe failure mode provided by the new hybrid composite materials.

## 4. Conclusions

The following conclusions were drawn from the presented study of bi-directional glass/carbon-epoxy hybrid composites:

- All tested configurations showed favourable pseudo-ductile stress-strain responses with a detectable damage initiation point and a wide margin before final failure, which is considered to be a safe failure mode compared to the usually abrupt fracture of conventional composite laminates.
- Elastic modulus increments in the range of 20–70% to the predicted modulus of the glass/epoxy baseline composite with the same structure (i.e. ply orientations) were achieved, together with a change from sudden to a safe, progressive failure mode.
- The damage initiation points of the different configurations were controlled by the fracture of the low strain material in the hybrid laminates (i.e. carbon/epoxy), which can be considered as a reference to define design limits for the new type hybrids.
- All tested laminate types provided a clear indication of damage initiation and accumulation visible to the naked eye, which is an additional safety feature of the developed hybrid composites. This can be exploited in critical structural applications and represent significant added value.
- The manufacturing of the developed laminates was found to be suitable for implementation in an industrial environment with no special requirements or equipment.

## CRediT authorship contribution statement

**Gergely Czél:** Conceptualization, Experiment execution and evaluation, Funding acquisition, Methodology, Writing – original draft.

## Declaration of competing interest

The authors declare that they have no known competing financial interests or personal relationships that could have appeared to influence the work reported in this paper.

## Acknowledgement

The research reported in this paper was supported by the National Research, Development and Innovation Office (NRDI, Hungary) through grants OTKA FK 131882 and TKP2020 IES, Grant No. BME-IE-NAT the latter based on the charter of bolster issued by the NRDI Office under the auspices of the Ministry for Innovation and Technology (Hungary). Gergely Czél is grateful for funding through the Premium Postdoctoral Fellowship Programme of the Hungarian Academy of Sciences. Thanks to Frederik Ohlsson and Oxeon for kindly providing the tape fabrics, and Ábel Pintér for his help with the experiments.

## References

[1] Wang Cheng, Zhang Shuai, Zhang Longfei, Xub Yewei, Zhang Lin. Evading the strength–ductility trade-off dilemma of rigid thermosets by incorporating triple crosslinks of varying strengths. Polym Chem 2020;11:6281–7. https://doi.org/10.1039/D0PY00928H.

[2] Swolfs Y, Gorbatikh L, Verpoest I. Fibre hybridisation in polymer composites: a review. Compos Appl Sci Manuf 2014;67:181–200. https://doi.org/10.1016/j.compositesa.2014.08.027.

[3] Wei Yujie, Li Yongqiang, Zhu Lianchun, Liu Yao, Lei Xianqi, Wang Gang, Wu Yanxin, Mi Zhenli, Liu Jiabin, Wang Hongtao, Gao Huajian. Evading the strength–ductility trade-off dilemma in steel through gradient hierarchical nanotwins. Nat Commun 2014;5:3580. https://doi.org/10.1038/ncomms4580.

[4] Swolfs Y, Shi J, Meerten Y, Hine P, Ward I, Verpoest I, Gorbatikh L. The importance of bonding in intralayer carbon fibre/self-reinforced polypropylene hybrid composites. Compos Appl Sci Manuf 2015;76:299–308. https://doi.org/10.1016/j.compositesa.2015.06.017.

[5] Jones RM. Design of composite structures. Blacksburg: Bull ridge publishing; 2015.

[6] Ou Y, González C, Vilatela JJ. Interlaminar toughening in structural carbon fiber/epoxy composites interleaved with carbon nanotube veils. Compos Appl Sci Manuf 2019;124:105477. https://doi.org/10.1016/j.compositesa.2019.105477.

[7] Kostagiannakopoulou C, Tsilimigkra X, Sotiriadis G, Kostopoulos V. Synergy effect of carbon nano-fillers on the fracture toughness of structural composites. Compos B Eng 2017;129:18–25. https://doi.org/10.1016/j.compositesb.2017.07.012.

[8] Romhány G, Szebényi G. Interlaminar crack propagation in MWCNT/fiber reinforced hybrid composites. Express Polym Lett 2009;3:145–51. https://doi.org/10.3144/expresspolymlett.2009.19.

[9] Romhány G, Szebényi G. Interlaminar fatigue crack growth behavior of MWCNT/carbon fiber reinforced hybrid composites monitored via newly developed acoustic emission method. Express Polym Lett 2012;6:572–80. https://doi.org/10.3144/expresspolymlett.2012.60.

[10] Turcsán T, Mészáros L. Mechanical performance of hybrid thermoset composites: effects of matrix and reinforcement hybridization. Compos Sci Technol 2017;141:32–9. https://doi.org/10.1016/j.compscitech.2017.01.005.

[11] Palazzetti R, Zucchelli A. Electrospun nanofibers as reinforcement for composite laminates materials – a review. Compos Struct 2017;182:711–27. https://doi.org/10.1016/j.compstruct.2017.09.021.

[12] Koprivova B, Lisnenko M, Solarska-Sciuk K, Prochazkova R, Novotny V, Mullerova J, Mikes P, Jencova V. Large-scale electrospinning of poly (Vinylalcohol) nanofibers incorporated with platelet-derived growth factors. Express Polym Lett 2020;14:987–1000. https://doi.org/10.3144/expresspolymlett.2020.80.

[13] Molnár K, Košťáková E, Mészáros L. The effect of needleless electrospun nanofibrous interleaves on mechanical properties of carbon fabrics/epoxy laminates. Express Polym Lett 2014;8:62–72. https://doi.org/10.3144/expresspolymlett.2014.8.

[14] Salehi MM, Hakkak F, Sadati Tilebon SM, Ataeefard M, Rafizadeh M. Intelligently optimized electrospun polyacrylonitrile/poly(vinylidene fluoride) nanofiber: using artificial neural networks. Express Polym Lett 2020;14:1003–17. https://doi.org/10.3144/expresspolymlett.2020.82.

[15] Lomov SV, Molnár K. Compressibility of carbon fabrics with needleless electrospun PAN nanofibrous interleaves. Express Polym Lett 2016;10:25–35. https://doi.org/10.3144/expresspolymlett.2016.4.

[16] Molnár K. Shear-aided annular needleless electrospinning. Mater Res Express 2019;6:075304. https://doi.org/10.1088/2053-1591/ab11fd.

[17] He HJ, Kara Y, Molnar K. In situ viscosity-controlled electrospinning with a low threshold voltage. Macromol Mater Eng 2019;4:1900349. https://doi.org/10.1002/mame.201900349.

[18] Boncel S, Rajyashree M, Sundaram RM, Windle AH, Koziol KKK. Enhancement of the mechanical properties of directly spun CNT fibers by chemical treatment. ACS Nano 2011;5:9339–44. https://doi.org/10.1021/nn202685x.

[19] Shamsuddin RR, Lee KY, Bismarck A. Ductile unidirectional continuous rayon fibre-reinforced hierarchical composites. Compos Appl Sci Manuf 2016;90. https://doi.org/10.1016/j.compositesa.2016.08.021. 663-641.

[20] Allaer K, De Baere I, Lava P, Van Paepegem W, Degrieck J. On the in-plane mechanical properties of stainless steel fibre reinforced ductile composites. Compos Sci Technol 2014;100:34–43. https://doi.org/10.1016/j.compscitech.2014.05.009.

[21] Callens MG, Gorbatikh L, Verpoest I. Ductile steel fibre composites with brittle and ductile matrices. Compos Appl Sci Manuf 2014;61:235–44. https://doi.org/10.1016/j.compositesa.2014.02.006.

[22] Callens MG, Gorbatikh L, Bertels E, Goderis B, Smet M, Verpoest I. Tensile behaviour of stainless steel fibre/epoxy composites with modified adhesion. Compos Appl Sci Manuf 2015;69:208–18. https://doi.org/10.1016/j.compositesa.2014.11.022.

[23] Callens MG, De Cuyper P, Gorbatikh L, Verpoest I. Effect of fibre architecture on the tensile and impact behaviour of ductile stainless steel fibre polypropylene composites. Compos Struct 2015;119:528–33. https://doi.org/10.1016/j.compstruct.2014.09.028.

[24] Fuller JD, Wisnom MR. Pseudo-ductility and damage suppression in thin ply CFRP angle-ply laminates. Compos Part A Appl Sci Manuf 2015;69:64–71. https://doi.org/10.1016/j.compositesa.2014.11.004.

[25] Yuan Y, Wang S, Yang H, Yao X, Liu B. Analysis of pseudo-ductility in thin-ply carbon fiber angle-ply laminates. Compos Struct 2017;180:876–82. https://doi.org/10.1016/j.compstruct.2017.08.070.

[26] Fuller JD, Wisnom MR. Exploration of the potential for pseudo-ductility in thin ply CFRP angle-ply laminates via an analytical method. Compos Sci Technol 2015;112:8–15. https://doi.org/10.1016/j.compscitech.2015.02.019.

[27] Yu H, Longana ML, Jalalvand M, Wisnom MR, Potter KD. Pseudo-ductility in intermingled carbon/glass hybrid composites with highly aligned discontinuous fibres. Compos Appl Sci Manuf 2015;73:35–44. https://doi.org/10.1016/j.compositesa.2015.02.014.

[28] Longana ML, Yu H, Lee J, Pozegic TR, Huntley S, Rendall T, Potter KD, Hamerton I. Quasi-isotropic and pseudo-ductile highly aligned discontinuous fibre composites

manufactured with the HiPerDiF (high performance discontinuous fibre) technology. Materials 2019;12:1794. https://doi.org/10.3390/ma12111794.
[29] Czél G, Pimenta S, Wisnom MR, Robinson P. Demonstration of pseudo-ductility in unidirectional discontinuous carbon fibre/epoxy prepreg composites. Compos Sci Technol 2015;106:110–9. https://doi.org/10.1016/j.compscitech.2014.10.022.
[30] Czél G, Jalalvand M, Wisnom MR. Design and characterisation of advanced pseudo-ductile unidirectional thin-ply carbon/epoxy-glass/epoxy hybrid composites. Compos Struct 2016;143:362–70. https://doi.org/10.1016/j.compstruct.2016.02.010.
[31] Czél G, Jalalvand M, Wisnom MR, Czigány T. Design and characterisation of high performance, pseudo-ductile all-carbon/epoxy unidirectional hybrid composites. Compos B Eng 2017;111:348–56. https://doi.org/10.1016/j.compositesb.2016.11.049.
[32] Czél G, Rev T, Jalalvand M, Fotouhi M, Longana ML, Nixon-Pearson OJ, Wisnom MR. Pseudo-ductility and reduced notch sensitivity in multi-directional all-carbon/epoxy thin-ply hybrid composites. Compos Appl Sci Manuf 2018;104:151–64. https://doi.org/10.1016/j.compositesa.2017.10.028.
[33] Fotouhi M, Jalalvand M, Saeedifar M, Xiao B, Wisnom MR. High performance quasi-isotropic thin-ply carbon/glass hybrid composites with pseudo-ductile behaviour loaded off-axis. Compos Struct 2020;247:112444. https://doi.org/10.1016/j.compstruct.2020.112444.
[34] Rev T, Jalalvand M, Fuller J, Wisnom MR, Czél G. A simple and robust approach for visual overload indication - UD thin-ply hybrid composite sensors. Compos Appl Sci Manuf 2019;121:376–85. https://doi.org/10.1016/j.compositesa.2019.03.005.
[35] Wisnom M, Potter K, Czél G, Jalalvand M. Strain overload sensor. no. GB2544792B. 2020. UK patent.
[36] Czél G, Wisnom MR. Demonstration of pseudo-ductility in high performance glass-epoxy composites by hybridisation with thin-ply carbon prepregs. Compos Appl Sci Manuf 2013;52:23–30. https://doi.org/10.1016/j.compositesa.2013.04.006.
[37] Wisnom MR, Czél G, Swolfs Y, Jalalvand M, Gorbatikh L, Verpoest I. Hybrid effects in thin ply carbon/glass unidirectional laminates: accurate experimental determination and prediction. Compos Appl Sci Manuf 2016;88:131–9. https://doi.org/10.1016/j.compositesa.2016.04.014.